

Skyrme random-phase approximation analysis of low-energy dipole states in oxygen isotopes

Tsunenori Inakura¹ and Yasuhiro Togano²

¹*Department of Physics, Faculty of Science, Niigata University, Niigata 950-2181, Japan*

²*Department of Physics, Rikkyo University, Tokyo 171-8501, Japan*



(Received 27 September 2017; revised manuscript received 17 January 2018; published 30 May 2018)

Low-energy dipole states in oxygen isotopes are investigated using a Hartree-Fock plus random-phase approximation calculation with Skyrme interactions. We obtain the lowest energy dipole state as isoscalar dominant on the spherical ground states of $^{16-22}\text{O}$, while that in ^{24}O couples to the continuum states. This suggests that the nature of low-energy dipole mode in light nuclei changes at $N = 16$.

DOI: [10.1103/PhysRevC.97.054330](https://doi.org/10.1103/PhysRevC.97.054330)

I. INTRODUCTION

The low-energy dipole (LED) state is one of the key ingredients to investigate the properties of nuclear excitations, and has attracted attention in connection with neutron stars, nucleosynthesis, the nuclear equation of state, and so on. The LED state appears around neutron separation energy S_n , having sizable strength up to several percent of the Thomas-Reiche-Kuhn sum rule, especially in unstable nuclei. It has been observed in many mass regions, e.g., ^{48}Ca [1], ^{68}Ni [2], ^{90}Zr [3], ^{132}Sn [4], and ^{208}Pb [5].

It was found from recent experiments [6–10] that the LED state in medium-mass and heavy-mass nuclei has two components. The lower-energy component has isoscalar (IS) plus isovector (IV) character, whereas the higher-energy component has IV dominant character. This phenomenon is called the isospin splitting of LED, and recently it was suggested that the LED isospin splitting holds in an unstable light nucleus [11].

LED states are often interpreted as collective oscillation of the neutron skin and the remnant core [12,13], which is IS dominant. However, its nature is still under debate. Reference [14] implies that the strong IV character of LEDs (IV-LEDs) is due to the coupling to the continuum in light neutron-rich nuclei. Although there have been many theoretical studies [15–18] devoted to clarify the properties of LED, the underlying structure of the LED isospin splitting is not well understood yet.

A recent experiment [11] confirmed that in ^{20}O there are two dipole states, at 5.36(5) and 6.84(7) MeV below S_n , and showed that the lower-energy state has stronger IS character, namely the LED isospin splitting holds in ^{20}O . The random-phase approximation (RPA) calculation with Skyrme interactions was performed, and it produced one dipole state having IS character, which is made from proton excitations rather than neutron excitations. LED states are observed in $^{14-20}\text{O}$ [11,19–24], and the lowest energy dipole state in ^{16}O is known to be IS dominant. Shell model calculations [22,25,26] produce LEDs, but their properties are not discussed.

To investigate nature of the LED in oxygen isotopes in connection with the LED isospin splitting, we study LEDs of

$^{14-24}\text{O}$ using a Skyrme-RPA calculation by focusing on the neutron number dependence of the LED isospin character. While the RPA calculation has difficulty in describing excitations of light nuclei in which the cluster correlation plays important roles, the preceding RPA calculation [27] succeeded in reproducing the lowest energy dipole state of ^{16}O . We apply the RPA calculation to $^{14-24}\text{O}$ after confirming its applicability and limitation. The pairing correlation is neglected in this paper. Although the pairing correlation would change shapes of ground states and cause accompanying rearrangement of the dipole excitation modes, it does not produce additional dipole excitations [28], unlike the quadrupole excitation. We simulate the effect of the pairing correlation by taking spherical ground states that the pairing correlation prefers.

The manuscript is organized as follows: Section II reviews briefly the Hartree-Fock (HF) and RPA calculation. In Sec. III, we analyze LED in oxygen isotopes. First, we calculate LEDs in ^{16}O and compare results with the experimental data in order to confirm applicability and limitations of the Skyrme-RPA calculation for oxygen isotopes. While the previous RPA calculation in Ref. [11] was performed with the deformed ground state, the present calculation is done with the spherical ground state. With the present calculation, we suggest another interpretation of the observed dipole states in ^{20}O . We follow with a discussion of the neutron number dependence of the LED structure for the oxygen isotopes. Conclusions are given in Sec. IV. A part of the result was reported in Ref. [11].

II. METHOD

We employ the HF+RPA approach to describe excitation states of oxygen isotopes. The numerical code used in the present calculation is a revised version of the code developed in Ref. [29]. Here we recapitulate the HF+RPA formalism. For other details, we refer the readers to Ref. [29].

We use the Skyrme effective interaction. The pairing correlation is neglected. The adopted Skyrme interactions are SkM* [30], UNEDF1 [31], and SLy4 [32]. SkM* is one of the most used Skyrme interactions for nuclear structure calculations. UNEDF1 was recently designed to reproduce

various experimental data in a wide range of the nuclear chart. SLy4 was constructed to reproduce a theoretical equation of state [33] and some experimental data in a wide mass region, especially for neutron-rich nuclei.

The size of the RPA matrix is reduced by assuming the reflection symmetry of the ground state with respect to $x = 0$, $y = 0$, and $z = 0$ planes. We adopt the three-dimensional coordinate representation with uniform mesh spacing $h = 0.5$ fm within a sphere of radius $R_{\text{box}} = 20$ fm.

The $E1$ operator D is expressed as

$$D = \frac{N}{A} \sum_{i \in p} r_i Y^{(1)}(\Omega_i) - \frac{Z}{A} \sum_{i \in n} r_i Y^{(1)}(\Omega_i), \quad (1)$$

after the center-of-mass correction. Here i is the index of nucleons and $i \in p$ ($i \in n$) indicates that the sum runs over protons (neutrons). The $E1$ strength from the ground state $|0\rangle$ to the excited state $|\alpha\rangle$ in an even-even nucleus is $B(E1; \alpha) = |\langle \alpha | D | 0 \rangle|^2$. For the one-particle–one-hole excitations, we calculate the transition amplitude $\langle \alpha | D | 0 \rangle$ within the HF+RPA. The same holds for the compressional IS dipole (ISD) operator D_{IS} ,

$$D_{\text{IS}} = \sum_{i \in p} r_i^3 Y^{(1)}(\Omega_i) + \sum_{i \in n} r_i^3 Y^{(1)}(\Omega_i). \quad (2)$$

The calculated excitation state is analyzed by use of particle-hole (ph) contribution C_{ph} and transition density $\delta\rho$. The ph contribution of an excitation from orbit i to orbit m is evaluated, with the forward and backward amplitudes $X_i(\mathbf{r})$ and $Y_i(\mathbf{r})$, as

$$C_{mi} = |X_{im}|^2 - |Y_{im}|^2, \quad (3)$$

in which X_{im} is extracted from $X_i(\mathbf{r})$ as

$$X_{im} = \int d\mathbf{r} \phi_m^*(\mathbf{r}) X_i(\mathbf{r}), \quad (4)$$

and similarly for Y_{im} . Here ϕ_m is m th wave function and the spin indices are omitted for simplicity. The transition density $\delta\rho$ is expressed as

$$\delta\rho(\mathbf{r}) = \sum_{i \in n, p} \{ \phi_i^*(\mathbf{r}) X_i(\mathbf{r}) + Y_i^*(\mathbf{r}) \phi_i(\mathbf{r}) \} \quad (5)$$

and the decomposed transition density regarding the ph excitation from i to m orbits, $\delta\rho_{i \rightarrow m}$, is calculated by

$$\delta\rho_{i \rightarrow m}(\mathbf{r}) = \phi_i^*(\mathbf{r}) \phi_m(\mathbf{r}) X_{im} + Y_{im}^* \phi_i(\mathbf{r}) \phi_m^*(\mathbf{r}). \quad (6)$$

The radial dipole transition density $\delta\rho_{L=1}(r)$ is calculated from $\delta\rho$ as

$$\delta\rho_{L=1}(r) = \int d\Omega r Y^{(1)}(\Omega) \delta\rho(\mathbf{r}). \quad (7)$$

In some cases, the transition density $\delta\rho$ and the ph contribution C_{ph} give different interpretations of excitations. The cause is as follows. The transition density is calculated as $\delta\rho \sim \sum_{\text{ph}} X_{\text{ph}} \phi_{\text{ph}}^* \phi_{\text{h}}$ (where we neglect Y_{ph} for simplicity). So, $\delta\rho$ is approximately of order $O(X_{\text{ph}})$, whereas the ph contribution $C_{\text{ph}} \sim |X_{\text{ph}}|^2$ is of order $O(X_{\text{ph}}^2)$. Combining the normalization condition $\sum_{\text{ph}} (|X_{\text{ph}}|^2 - |Y_{\text{ph}}|^2) = 1$, the ph excitations having small contributions to $\delta\rho$ are evaluated to be much smaller in the ph contribution C_{ph} . A typical

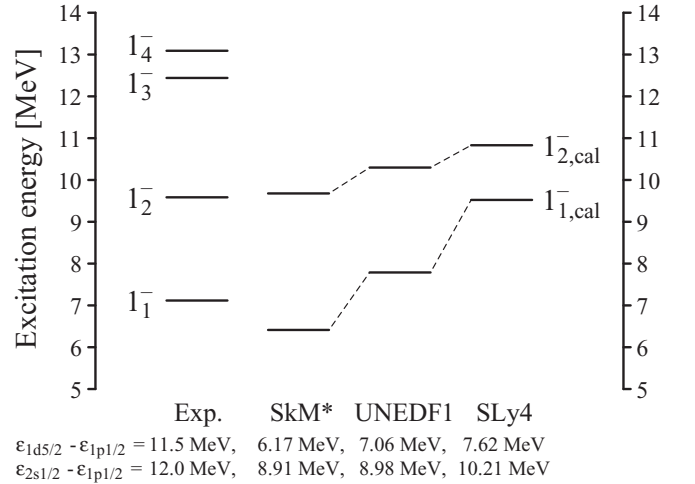


FIG. 1. Low-energy dipole states in ^{16}O , calculated with three Skyrme interactions, are compared with experimental values [34]. Observed proton single-particle level spacing [35] and calculated level spacing are shown at the bottom.

case is neutron emission mode; while a certain configuration exhausts almost unity of the ph contribution, $C_{\text{ph}} \sim 1$, both proton and neutron have non-negligible $\delta\rho$, which describes the remnant core receiving recoil motion. This characteristic feature becomes more noticeable approaching drip-line nuclei. Therefore, in order to appropriately investigate properties of calculated excitation states, we use both $\delta\rho$ and C_{ph} .

III. RESULTS AND DISCUSSION

A. Low-energy dipole excitation in ^{16}O

Figure 1 shows the calculated excitation energies of the LED states in ^{16}O with experimental data [34]. The excitation energy E_x , ISD energy-weighted sum rule (EWSR) fraction f_{ISD} [36], and $E1$ strength $B(E1)$ of observed 1^- states and calculated states 1_{cal}^- are listed in Table I. The calculated E_x of 1_{cal}^- states

TABLE I. Experimental and calculated excitation energy E_x , ISD EWSR fraction f_{ISD} , and dipole strength $B(E1)$ of low-energy dipole states in ^{16}O .

	E_x (MeV)	f_{ISD} (% of EWSR)	$B(E1)$ ($e^2\text{fm}^2$)
Experimental data in ^{16}O			
1_1^-	7.11685(14)	4.2	$1.5(1) \times 10^{-4}$
1_2^-	9.585(11)		$2.7(5) \times 10^{-5}$
1_3^-	12.440(2)		$5.7(8) \times 10^{-3}$
1_4^-	13.090(8)		$1.3(2) \times 10^{-2}$
$1_{1,\text{cal}}^-$ state in ^{16}O			
SkM*	6.41	1.25	3.6×10^{-4}
UNEDF1	7.79	1.67	5.4×10^{-4}
SLy4	9.52	2.57	21.8×10^{-4}
$1_{2,\text{cal}}^-$ state in ^{16}O			
SkM*	9.68	0.008	5.09×10^{-2}
UNEDF1	10.30	0.006	3.16×10^{-2}
SLy4	10.83	0.016	5.85×10^{-2}

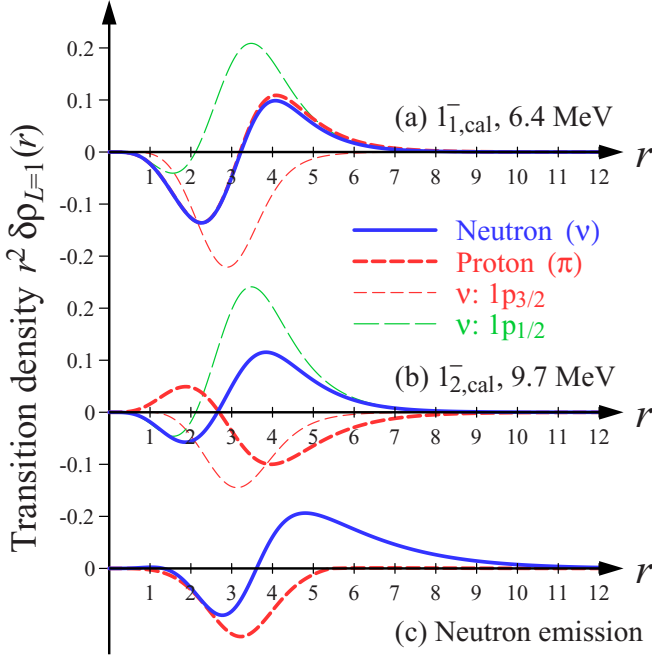


FIG. 2. Radial transition densities $r^2 \delta \rho_{L=1}(r)$ of $1^-_{1,\text{cal}}$, $1^-_{2,\text{cal}}$ states, and neutron emission mode in ^{16}O , calculated with the SkM* interaction. Thick solid blue and thick dashed red lines denote neutron and proton transition densities. Thin dashed red and thin long-dashed green lines denote neutron transition densities decomposed to $1p_{3/2}$ and $1p_{1/2}$ hole orbits, respectively.

are scattered depending on the interactions used. Differences of the calculated E_x of $1^-_{1,\text{cal}}$ states come from the level spacing of the single-particle energies ε , denoted in the bottom of Fig. 1. Narrower level spacing produces lower excitation energy. The calculated f_{ISD} are smaller than experimental data, while the $B(E1)$ values are overestimated. This trend is also seen in other RPA calculations [27].

The transition densities of the $1^-_{1,\text{cal}}$ state calculated with SkM* are plotted in Fig. 2(a). Proton and neutron transition densities $\delta \rho^\pi$ and $\delta \rho^\nu$ are almost the same, indicating that this state is ISD, in which the proton and neutron act coherently. The transition densities have nodes at $r \sim 3.2$ fm, in good agreement with the measured transition density [20] as well as the preceding RPA calculation [27]. UNEDF1 and SLy4 interactions produce similar transition densities, as shown in Fig. 3 in which we plot the proton transition densities calculated with three Skyrme interactions. However, these well-reproduced transition densities give different f_{ISD} and

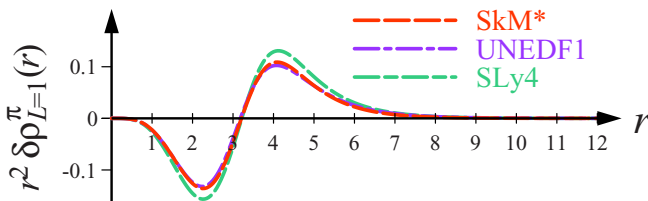


FIG. 3. Proton radial transition densities $r^2 \delta \rho_{L=1}^\pi(r)$ of $1^-_{1,\text{cal}}$ states calculated with SkM*, UNEDF1, and SLy4 interactions.

TABLE II. Calculated particle-hole contributions C_{ph} of $1^-_{1,\text{cal}}$ and $1^-_{2,\text{cal}}$ states in ^{16}O .

	SkM*	UNEDF1	SLy4
$1^-_{1,\text{cal}}$ state in ^{16}O			
$\nu : 1p_{1/2} \rightarrow 2s_{1/2}$	0.416	0.391	0.322
$\nu : 1p_{3/2} \rightarrow 1d_{5/2}$	0.031	0.034	0.029
$\nu : 1p_{3/2} \rightarrow 1d_{3/2}$	0.016	0.021	0.013
$\pi : 1p_{1/2} \rightarrow 2s_{1/2}$	0.455	0.479	0.561
$\pi : 1p_{3/2} \rightarrow 1d_{5/2}$	0.031	0.035	0.038
$\pi : 1p_{3/2} \rightarrow 1d_{3/2}$	0.012	0.014	0.014
$1^-_{2,\text{cal}}$ state in ^{16}O			
$\nu : 1p_{1/2} \rightarrow 2s_{1/2}$	0.488	0.494	0.581
$\nu : 1p_{3/2} \rightarrow 1d_{5/2}$	0.014	0.014	0.022
$\nu : 1p_{3/2} \rightarrow 1d_{3/2}$	0.009	0.012	0.014
$\pi : 1p_{1/2} \rightarrow 2s_{1/2}$	0.464	0.435	0.357
$\pi : 1p_{3/2} \rightarrow 1d_{5/2}$	0.011	0.007	0.008
$\pi : 1p_{3/2} \rightarrow 1d_{3/2}$	0.006	0.004	0.005

$B(E1)$ values (see Table I). This differential can be explained as follow. The f_{ISD} (i.e., ISD strength) and $B(E1)$ are obtained as the radial integral of the transition density. Since the transition density has a negative part up to the node (~ 3 fm) and positive part above the node as shown in Fig. 3, the small difference in the transition density leads the large difference in f_{ISD} or $B(E1)$ values.

In Fig. 2(a), we also plot the neutron transition densities decomposed to $1p_{3/2}$ and $1p_{1/2}$ hole states, $\delta \rho_{1p_{3/2}}^\nu$ and $\delta \rho_{1p_{1/2}}^\nu$. Those for protons are not plotted since they are almost identical to neutrons. Both of $\delta \rho_{1p_{3/2}}^\nu$ and $\delta \rho_{1p_{1/2}}^\nu$ have sizable but out-of-phase contributions to $\delta \rho^\nu$. More detailed analysis of the transition densities decomposed to ph excitations shows that $\delta \rho_{1p_{3/2}}^\nu$ is made from three ph excitations, from $1p_{3/2}$ to $1d_{5/2}$, $1d_{3/2}$, and continuum states, all of which have quantitative and coherent contributions, while $\delta \rho_{1p_{1/2}}^\nu$ is made mainly from one excitation, $1p_{1/2} \rightarrow 2s_{1/2}$. It is instructive to point out that these contributions to $\delta \rho$ are apparently different from the ph contributions C_{ph} shown in Table II, in which we list the three largest C_{ph} values for the proton and neutron. The neutron and proton $1p_{1/2} \rightarrow 2s_{1/2}$ excitations exhaust a large fraction of the contribution, ~ 0.87 , and the ph contributions related to $1p_{3/2}$ states are rather small, irrespective of the Skyrme interactions. Even summed ph contributions from $1p_{3/2}$ states to all particle states of the proton and neutron carry $C_{\text{ph}} \sim 0.1$ only, although $\delta \rho_{1p_{3/2}}^\nu$ and $\delta \rho_{1p_{1/2}}^\nu$ have comparable contributions to $\delta \rho$.

The observed 1^-_2 state at 9.585(11) MeV is known to be $^{12}\text{C} + \alpha$ cluster state [37–44]. The RPA calculation does not describe such a cluster state. The calculated second lowest dipole state $1^-_{2,\text{cal}}$ appears at ~ 10 MeV, with an IV dipole character. Similar to the $1^-_{1,\text{cal}}$ state, the decomposed transition densities $\delta \rho_{1p_{3/2}}^\nu$ and $\delta \rho_{1p_{1/2}}^\nu$ have large contributions with opposite signs [Fig. 2(b)], and the main ph excitations are $1p_{1/2} \rightarrow 2s_{1/2}$ excitations of the proton and neutron (Table II). On the other hand, in contrast to the $1^-_{1,\text{cal}}$ state, the $1^-_{2,\text{cal}}$ state has negligibly small f_{ISD} and large $B(E1)$ as shown in Table I. This $1^-_{2,\text{cal}}$ state is considered to correspond to the 1^-_4 state at $E_x = 13.090(8)$ MeV which has IV character and large

spectroscopic factors of $1p_{3/2}$ and $1p_{1/2}$ orbits [45,46]. Since Skyrme interactions underestimate the level spacing of $1p_{1/2}$ and $1d_{5/2}$, $2s_{1/2}$ orbits (see bottom of Fig. 1), the calculated excitation energy of the $1_{2,\text{cal}}^-$ state is lower by a few MeV than that of the observed 1_4^- state. The main difference between the $1_{1,\text{cal}}^-$ and $1_{2,\text{cal}}^-$ states is that the proton and neutron act in phase or out of phase, i.e., they have IS or IV character. This isospin behavior is consistent with the LED isospin splitting observed in the experiments: the lower-energy (higher-energy) component has stronger IS (IV) character.

It is worthwhile to note that the nucleon emission mode has a transition density which is different from those to the bound excited states. An example is shown in Fig. 2(c), in which we plot the transition density of the neutron emission mode appearing at 14.4 MeV with an adjusted vertical scale for comparison. Inside the nucleus, the proton and neutron move coherently while only the neutron has a large transition density outside. These transition densities apparently resemble those of the so-called pygmy dipole resonance, i.e., collective oscillation of the neutron skin and the remnant core, but $\delta\rho^v$ has a long tail which comes up to $r \gtrsim 10$ fm. This slow damping of $\delta\rho^v$ reflects the neutron excitation to the continuum state which is expressed by the plane waves. Also the neutron emission mode has a characteristic C_{ph} , that is, a certain excitation to the continuum state exhausts almost unity. In the present case, the neutron excitation of $1p_{1/2} \rightarrow$ continuum states carries $C_{\text{ph}} = 0.93$. Therefore we can identify nucleon emission mode from $\delta\rho$ and C_{ph} .

As a summary of ^{16}O calculations, the Skyrme-RPA calculation fairly reproduces the properties of 1_1^- state, i.e., the ISD state, and produces the LED isospin splitting. However, it is difficult to reproduce excitation energies E_x of LEDs, which are sensitive to the single-particle levels. And, as is known, the RPA calculation does not describe many-particle–many-hole states, including cluster structure.

B. Low-energy dipole excitation in ^{20}O

Next, we move to the LED states in ^{20}O to interpret the result obtained in Ref. [11]. The Skyrme-HF calculations produce a prolately deformed ground state of ^{20}O with quadrupole deformation parameter $\beta_2 \sim 0.2$. The RPA calculation with SkM* on top of the deformed ground state gives one dipole state at 4.45 MeV below neutron threshold energy $|\lambda_n|$, which is defined from the neutron Fermi energy λ_n . Some of the results with this deformed ground state have been shown already in Ref. [11]. This 4.45 MeV dipole state couples the octupole mode due to deformation. This indicates that octupole states have some dipole strength in a deformed nucleus. In the ^{20}O case, the octupole state appears at 7.4 MeV with a small $B(E1)$ value. We neglect it since we pay our attention to the dipole state in this paper. The second lowest dipole excitation appearing at 8.7 MeV, which is above $|\lambda_n|$, is a neutron emission mode. The excitation energy E_x , ISD EWSR fraction f_{ISD} , $E1$ strength $B(E1)$, and neutron threshold energy $|\lambda_n|$ calculated with SkM* interaction are listed in Table III with experimental data. Here, although the deformation splits the dipole state into two states with an energy difference of a few tens keV, we treat them as one state and pick the $K = 0$

TABLE III. Properties of observed and calculated dipole states in ^{20}O . The SkM* interaction was used.

	E_x (MeV)	f_{ISD} (% of EWSR)	$B(E1)$ ($e^2\text{fm}^2$)	S_n or $ \lambda_n $ (MeV)
Expt. 1_1^-	5.36(5)	2.70(32)	$3.57(20) \times 10^{-2}$	7.608
Expt. 1_2^-	6.84(7)	0.67(12)	$3.79(26) \times 10^{-2}$	7.608
Deformed ^{20}O	4.45	0.23	0.72×10^{-2}	7.79
Spherical ^{20}O	6.52	0.51	0.11×10^{-2}	7.65

mode as representative since the experimental resolution was not enough to separate them [11]. The calculated dipole state has smaller f_{ISD} and larger $B(E1)$ than those of the 1_1^- state in ^{16}O . This tendency is consistent with the experimental data of ^{20}O and ^{16}O .

As displayed in Fig. 4(a), the transition density of the 4.45 MeV state shows that the state has IS character similar to the $1_{1,\text{cal}}^-$ state in ^{16}O . The proton and neutron transition densities have similar shapes to each other. Therefore, proton and neutron contributions to $\delta\rho$ are comparable. However, the ph contribution C_{ph} listed in Table IV claims that this state is made mainly by proton excitations. The proton excitation $[101]1/2 \rightarrow [220]1/2$ (energy difference is 4.4 MeV) has the largest ph contribution $C_{\text{ph}} = 0.59$. The decomposed transition density of this ph excitation is responsible for $\delta\rho^\pi$ outside the nucleus, $r \gtrsim 3$ fm. The second and third largest ph contributions are also proton excitations, whose transition densities contribute mainly at $r \lesssim 3$ fm. The neutron excitations carry only $C_{\text{ph}} = 0.022$ in total. It should be noted that, in the octupole state at 7.4 MeV, the neutron excitation $[101]1/2 \rightarrow [211]1/2$ carries the largest ph contribution $C_{\text{ph}} = 0.61$ in contrast to the dipole state at 4.45 MeV. UNEDF1 and SLy4 interactions give similar results: One LED state with IS character (IS-LED) appears below $|\lambda_n|$ and the largest ph contribution

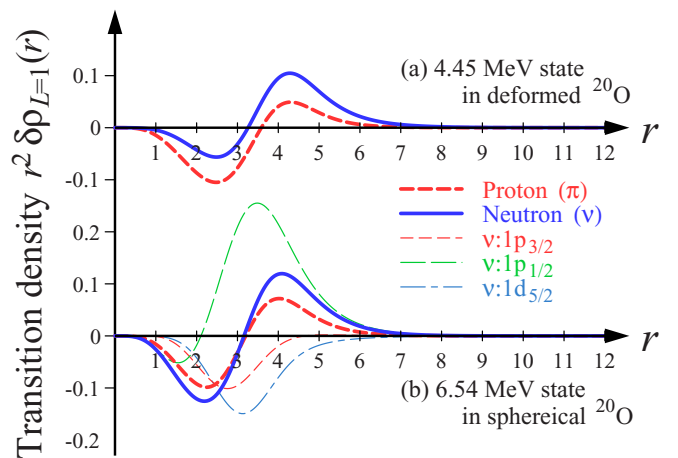


FIG. 4. Radial transition densities $r^2\delta\rho_{L=1}(r)$ of (a) the 4.45 MeV state obtained on the deformed ground state and (b) the 6.54 MeV state obtained on the spherical ground state. Thick lines denote proton and neutron transition densities and thin lines neutron decomposed transition densities. The SkM* interaction was used. See text for details.

TABLE IV. Particle-hole contribution C_{ph} of the calculated LED states in deformed and spherical ^{20}O . The SkM* interaction was used. See text for details.

Deformed ^{20}O		Spherical ^{20}O	
$\pi : [101]1/2 \rightarrow [220]1/2$	0.593	$\nu : 1p_{1/2} \rightarrow 2s_{1/2}$	0.648
$\pi : [101]1/2 \rightarrow [211]1/2$	0.188	$\pi : 1p_{1/2} \rightarrow 2s_{1/2}$	0.225
$\pi : [101]1/2 \rightarrow [200]1/2$	0.176	$\pi : 1p_{3/2} \rightarrow 1d_{5/2}$	0.018
$\nu : [101]1/2 \rightarrow [211]1/2$	0.016	$\nu : 1d_{5/2} \rightarrow 1f_{7/2}$	0.014
$\pi : [110]1/2 \rightarrow [200]1/2$	0.003	$\pi : 1p_{3/2} \rightarrow 1d_{3/2}$	0.011
$\pi : [110]1/2 \rightarrow [220]1/2$	0.002	$\nu : 1p_{3/2} \rightarrow 1d_{5/2}$	0.011
$\pi : [110]1/2 \rightarrow [211]1/2$	0.001	$\nu : 1p_{1/2} \rightarrow 1d_{5/2}$	0.009

is carried by the proton excitation $[101]1/2 \rightarrow [220]1/2$ with $C_{\text{ph}} \sim 0.6$.

The shell model calculation [22] produces four 1^- states below excitation energy 8 MeV in ^{20}O . Using a weak-coupling model with a simple ph interaction [47,48], we expect that two lower 1^- states are the proton excitation $^{15}\text{N}(\text{g.s.}) \times ^{21}\text{F}(\frac{1}{2}^+)$ and the neutron excitation $^{15}\text{O}(\text{g.s.}) \times ^{21}\text{O}(\frac{1}{2}^+)$ and that the next two 1^- states are coupling states of the $1p_{1/2}$ hole state to the lowest $\frac{3}{2}^+$ states in ^{21}O and ^{21}F . This proton excitation $^{15}\text{N}(\text{g.s.}) \times ^{21}\text{F}(\frac{1}{2}^+)$ would correspond to our resulting dipole state at 4.45 MeV, in which the main ph excitation is $[101]1/2 \rightarrow [220]1/2$ of the proton.

The HF+RPA calculations are performed without pairing correlation. While the pairing correlations tend to form the spherical shape, they have small impact on the dipole excitation [28]. Since the HF+BCS and Hartree-Fock-Bogoliubov (HFB) calculations [28,49] produce the spherical ground state of ^{20}O and the experimental data also prefer the spherical one, we also perform the RPA calculation on the spherical ground state. The spherical ground state is produced by the constrained HF calculation. The center-of-mass motion, which is an indicator for accuracy of self-consistency of the RPA calculations, appears at the imaginary energy $0.04i$ MeV, close to zero energy with the SkM* interaction. One LED state is obtained below $|\lambda_n|$ on the spherical ground state. The bottom row of Table III shows properties of this LED state. Compared with the deformed case, higher E_x , larger f_{ISD} , and smaller $B(E1)$ are obtained. Its transition density, shown in Fig. 4(b), is quite similar to that of $1_{1,\text{cal}}^-$ state in ^{16}O , other than the different amplitudes of $\delta\rho^\nu$ and $\delta\rho^\pi$ coming from $N > Z$, showing the IS character of this state.

The decomposed transition densities [Fig. 4(b)] and the ph contribution C_{ph} (right column in Table IV) exhibit similarity between this LED state in spherical ^{20}O and the $1_{1,\text{cal}}^-$ state in ^{16}O . The largest ph contributions are carried by the proton and neutron excitations $1p_{1/2} \rightarrow 2s_{1/2}$. Reflecting the difference of level spacing of $1p_{1/2}$ and $2s_{1/2}$ orbits in spherical ^{20}O , 9.0 MeV for the neutron and 11.0 MeV for the proton, the neutron ph contribution is larger than that of the proton. The second largest proton ph contribution is carried by the $1p_{3/2} \rightarrow 1d_{5/2}$ excitation, the same as that in ^{16}O . Since the neutron $1d_{5/2}$ orbit is partially occupied in ^{20}O , the $1p_{3/2} \rightarrow 1d_{5/2}$ excitation is hindered and the $1d_{5/2} \rightarrow 1f_{7/2}$ excitation has the second

largest neutron ph contribution. The neutron $1d_{5/2} \rightarrow 1f_{7/2}$ excitation contributes to $\delta\rho$, compensating for the contribution of the neutron $1p_{3/2} \rightarrow 1d_{5/2}$ excitation which is suppressed in ^{20}O . As a result, the transition density of the LED state in spherical ^{20}O is similar to that of the $1_{1,\text{cal}}^-$ state in ^{16}O .

In the cases of both the deformed and spherical ground states, IS-LEDs appear below $|\lambda_n|$. However, they exhibit very different ph contributions C_{ph} . In the deformed case, the dipole state is made by proton excitations with summed ph contribution $\sum_\pi C_{\text{ph}} = 0.98$ while, in the spherical case, it is made by neutron excitations with $\sum_\nu C_{\text{ph}} = 0.73$. It is not clear what causes this discrepancy. This problem must be solved but it is beyond our scope in this paper.

UNEDF1 produces an IS-LED on spherical ^{20}O at 7.1 MeV. Even though its excitation energy is higher than $|\lambda_n|$, the IS-LED decouples well from the neutron emission mode. Its transition density is similar to those calculated with SkM*. The largest ph contributions are carried by the neutron $1p_{1/2} \rightarrow 2s_{1/2}$ excitation, $C_{\text{ph}} = 0.82$, and the second largest by the proton $1p_{1/2} \rightarrow 2s_{1/2}$ excitation, $C_{\text{ph}} = 0.09$. SLy4 also produces an IS-LED above $|\lambda_n|$, but one which couples with neutron emission modes.

The Skyrme-RPA produces one IS-LED around $|\lambda_n|$ whereas two dipole states are observed below S_n [11]. If we deepen the attractive potential by multiplying the parameter t_0 in the Skyrme interaction SkM* by a factor 1.04, we obtain an IV-LED state appearing below $|\lambda_n|$, which resembles the $1_{2,\text{cal}}^-$ state in ^{16}O . This suggests that this IV-LED state can be interpreted as the LED isospin splitting partner of the low-energy ISD state.

From the discussions above, we have three inferences on the IV-LED state as the LED isospin splitting partner. (1) As shown by deepening the potential, the calculated higher-energy IV state can be the LED isospin splitting partner. (2) The partner could not be reproduced by the present calculation. (3) One of the observed dipole states in ^{20}O has a complex structure which the present calculation cannot describe. One possibility for the complex structure originates from the pairing correlation. The HFB and HF+BCS calculations result in a fractional occupation probability of the neutron $2s_{1/2}$ orbit and the RPA calculation does not deal with excitations from it. However, the canonical-basis time-dependent HFB calculation [50] gives only one dipole state below $|\lambda_n|$. Another possibility is connected with many-particle-many-hole excitation, which can be described by the shell model calculation and the second RPA (the extended RPA) calculation. Another possibility for the observed 1^- state is a cluster structure such as that of the $^{14}\text{C} + ^6\text{He}$ system [51].

C. Evolution of low-energy dipole state in oxygen isotopes

Let us examine LEDs in oxygen isotopes. Figure 5 gives the $E1$ and ISD transition up to excitation energy 12 MeV in $^{14-24}\text{O}$, calculated with the SkM* interaction on the spherical ground states. The $E1$ and ISD strengths are indicated by blue disks and open circles, respectively. The area of a disk or circle is proportional to the strength. The basic features of LEDs and how they evolve with neutron number N are clearly visible. The lowest energy dipole states in ^{14}O and ^{24}O appear above

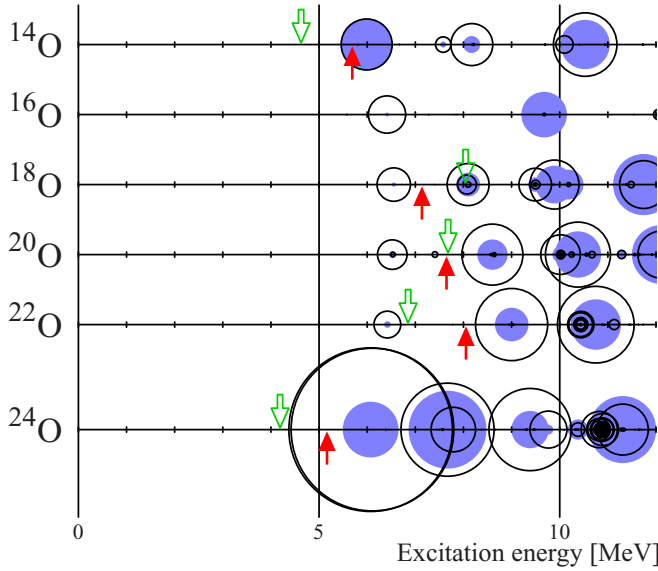


FIG. 5. $E1$ strengths and compressional isoscalar dipole strengths in $^{14-24}\text{O}$, represented by blue disks and open circles. Red arrows located below the horizontal axis denote the calculated proton (^{14}O) and neutron ($^{16-24}\text{O}$) threshold energies. Green open arrows located above the horizontal axis denote the experimentally known proton (^{14}O) and neutron ($^{16-24}\text{O}$) separation energies. See text for details.

$|\lambda_n|$ and have large $E1$ and ISD strengths. In $^{16-22}\text{O}$, the lowest energy dipole states appear at excitation energy ~ 6.5 MeV below $|\lambda_n|$, being insensitive to N . They are IS dominant states, and their ISD strengths decrease slightly as the neutron number N increases.

The transition densities of the lowest energy dipole states in $^{14-24}\text{O}$ are shown in Fig. 6. Those of $^{16,20}\text{O}$ are the same as in Figs. 2(a) and 4(b). The lowest energy dipole states in ^{14}O and ^{24}O have transition densities of the particle emission mode. It is clearly seen that the lowest energy dipole states in $^{16-22}\text{O}$ are IS-LEDs. The neutron transition density is not sensitive to the neutron number N , while the proton transition density is suppressed and shrinks with increasing N . This is related to the fact that the neutron single-particle energies of $1p_{1/2}$ and $2s_{1/2}$ orbits change only by ~ 1 MeV (and the level spacing changes only by 0.3 MeV) in shifting from ^{16}O to ^{22}O while the proton Fermi level $1p_{1/2}$ orbit deepens by 10 MeV.

In ^{14}O , the lowest energy dipole state appears at 6.0 MeV which is above the proton threshold energy $|\lambda_p| = 5.7$ MeV. Note that the observed 1_1^- state in ^{14}O appears at 5.17 MeV which is above the proton separation energy $S_p = 4.63$ MeV. As is seen in Fig. 6(a), this state is a proton emission mode. Since the nucleon emission mode contributes to both the IV and IS dipole modes, not only $E1$ but ISD strengths have large values. The calculated $B(E1)$ value, $0.064 e^2\text{fm}^2$, is very consistent with experimental data: $B(E1; \uparrow) = 0.064(12) e^2\text{fm}^2$ [21]. A large ISD strength is also observed [24]. These observables support our result that the lowest energy dipole state in ^{14}O is the proton emission mode.

Let us turn to the LED in ^{18}O . The results are similar to those of ^{20}O . The same as for ^{20}O , the ground state of ^{18}O is expected to be spherical [28,49], although the Skyrme-HF

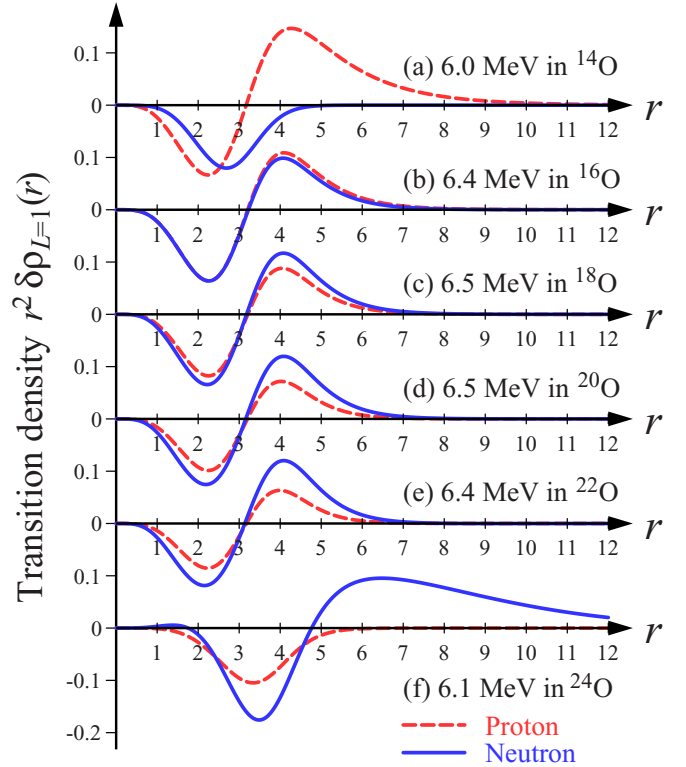


FIG. 6. Radial transition densities $r^2\delta\rho_{L=1}(r)$ of the lowest dipole modes in $^{16-22}\text{O}$. Solid and dashed lines denote neutron and proton transition densities, respectively. The SkM* interaction was used.

produces a deformed ground state with $\beta_2 = 0.15$. We perform the RPA calculations on the spherical ground state of ^{18}O . One ISD state is obtained at 6.5 MeV below $|\lambda_n|$, while three LEDs are observed at 4.4554(10), 6.19822(40), and 7.6159(7) MeV below S_n [34]. The properties of the calculated state are again similar to those of the ISD states on spherical ^{20}O and ^{16}O . The transition density displayed in Fig. 6(c) clearly shows the IS character. The neutron excitation $1p_{1/2} \rightarrow 2s_{1/2}$ has the largest ph contribution, $C_{\text{ph}} = 0.56$. The second largest ph contribution, $C_{\text{ph}} = 0.32$, is carried by the proton excitation $1p_{1/2} \rightarrow 2s_{1/2}$.

^{22}O is a semimagic nucleus in which the HF calculation produces a spherical ground state. The ISD excitation appears at 6.4 MeV below $|\lambda_n|$. The transition density shows IS character, as displayed in Fig. 6(e). The neutron excitation $1p_{1/2} \rightarrow 2s_{1/2}$ has the largest ph contribution, $C_{\text{ph}} = 0.73$. The second largest ph contribution, $C_{\text{ph}} = 0.18$, is carried by the proton excitation $1p_{1/2} \rightarrow 2s_{1/2}$. And the third largest is $C_{\text{ph}} = 0.02$ by the neutron excitation $1d_{5/2} \rightarrow 1f_{7/2}$. In ^{22}O , out-of-phase transition densities of neutron $1p_{1/2} \rightarrow 2s_{1/2}$ and $1d_{5/2} \rightarrow 1f_{7/2}$ excitations make the node at $r \sim 3$ fm.

In ^{24}O , since the neutron $2s_{1/2}$ orbit is occupied, the neutron excitation $1p_{1/2} \rightarrow 2s_{1/2}$ is not allowed. Due to the small number of resonant states, it is difficult to generate the neutron transition density having a node at $r \sim 3$ fm. Accordingly, the ISD state does not appear below $|\lambda_n|$ in ^{24}O . The lowest energy dipole state, which appears above $|\lambda_n|$, is the neutron emission

mode ($2s_{1/2} \rightarrow$ continuum states), as seen by its transition density, shown in Fig. 6(f).

The nature of the lowest energy dipole state in $^{16-22}\text{O}$ is common (in the present calculation), since the two largest ph contributions are always carried by the $1p_{1/2} \rightarrow 2s_{1/2}$ excitation of neutrons and protons in $^{16-22}\text{O}$. In addition, the nature of the LED is changed in the very proton/neutron-rich regions, ^{14}O and ^{24}O , as shown by the change of transition density to the particle emission mode. This is in line with the rapid increase of the IV component of LED at $N = 16$ calculated previously [14].

UNEDF1 produces IS-LED states on spherical ground states at excitation energies around $|\lambda_n|$ in $^{16-22}\text{O}$, which decouple from neutron emission mode. SLy4, which most overestimates the excitation energy of the ISD states in ^{16}O , also produces some IS-LED states around $|\lambda_n|$ on spherical ground states, but some of these strongly couple with the neutron emission mode.

The Skyrme-RPA with SkM* interaction produces one IS-LED state below $|\lambda_n|$ in $^{16-22}\text{O}$, whereas two or three LEDs are observed in $^{16-20}\text{O}$. Since the properties of the lowest energy dipole states in ^{16}O and ^{20}O are reproduced by the present RPA calculation, we think that one of the observed LEDs in $^{16-20}\text{O}$ corresponds to the calculated IS-LED state. In order to discuss the other LEDs, we should consider beyond-RPA effects such as the many-particle-many-hole excitation and/or the cluster correlation.

IV. CONCLUSION

We calculated LED states in oxygen isotopes using the HF+RPA approach with Skyrme interactions to clarify the properties of LEDs. The Skyrme-RPA calculation reproduces the LEDs in ^{16}O . The lower-energy state is ISD dominant and the higher-energy state has IV character, in coincidence with known LED isospin splitting in heavier nuclei. The calculated transition density of the $1_{1,\text{cal}}^-$ state agrees well with the experimental data, while the calculated ISD strength is underestimated.

The ISD state appears in $^{16-22}\text{O}$ below or close to the neutron threshold energy $|\lambda_n|$. In $^{18,20}\text{O}$, the HF produces deformed ground states whereas the HFB calculation and experimental data prefer spherical ones. The RPA calculations on both the deformed and spherical ground states give ISD states, but the particle-hole excitations having large contributions strongly depend on the shape of the ground state. For the deformed (spherical) ground state, proton (neutron) excitations are dominant. For all calculated ISD states on the spherical ground states in $^{16-22}\text{O}$, the transition densities are quite similar to each other, showing clear IS character. The particle-hole excitations having the largest contributions are $1p_{1/2} \rightarrow 2s_{1/2}$ of the proton and neutron. Since the $2s_{1/2}$ orbit is occupied in ^{24}O , the ISD state does not appear below $|\lambda_n|$ in ^{24}O .

We obtained only one LED at excitation energy $\lesssim |\lambda_n|$ in $^{18-22}\text{O}$, while two or three dipole states are observed experimentally. The LED which would correspond to the higher-energy component of the LED isospin splitting does not appear in the present calculations, since its excitation energy is higher than $|\lambda_n|$ and it may couple neutron emission modes, even if it exists. Since there is competition of collective excitation and cluster correlations in light nuclei, cluster model and shell model calculations are desired to clarify the nature of LEDs in light nuclei, which the RPA calculation fails to reproduce.

Our Skyrme-RPA calculations, combined with the results of Ref. [14], demonstrate that the LED mode in oxygen isotopes changes from the ISD mode to the neutron emission mode at $N = 16$, for which the $2s_{1/2}$ orbit is occupied. The present results help the deeper understanding of LED behavior in heavier neutron-rich nuclei, such as the LED isospin splitting and neutron number dependence of the LED properties.

ACKNOWLEDGMENTS

We thank M. Kimura for fruitful comments on cluster structure. This work is financially supported by a Grant-in-Aid for Scientific Research on Innovative Areas, Grants No. 24105005 and No. 24105008, by The Ministry of Education, Culture, Sports, Science and Technology, Japan.

-
- [1] T. Hartmann, M. Babilon, S. Kamenarich, E. Litvinova, D. Savran, S. Volz, and A. Zilges, *Phys. Rev. Lett.* **93**, 192501 (2004).
 - [2] O. Wieland *et al.*, *Phys. Rev. Lett.* **102**, 092502 (2009); D. M. Rossi *et al.*, *ibid.* **111**, 242503 (2013).
 - [3] C. Iwamoto *et al.*, *Phys. Rev. Lett.* **108**, 262501 (2012).
 - [4] P. Adrich *et al.*, *Phys. Rev. Lett.* **95**, 132501 (2005).
 - [5] A. Tamii *et al.*, *Phys. Rev. Lett.* **107**, 062502 (2011).
 - [6] D. Savran, M. Babilon, A. M. van den Berg, M. N. Harakeh, J. Hasper, A. Matic, H. J. Wörtche, and A. Zilges, *Phys. Rev. Lett.* **97**, 172502 (2006).
 - [7] J. Endres, D. Savran, A. M. van den Berg, P. Dendooven, M. Fritzsche, M. N. Harakeh, J. Hasper, H. J. Wörtche, and A. Zilges, *Phys. Rev. C* **80**, 034302 (2009).
 - [8] J. Endres *et al.*, *Phys. Rev. Lett.* **105**, 212503 (2010).
 - [9] V. Derya *et al.*, *Phys. Lett. B* **730**, 288 (2014).
 - [10] D. Negi *et al.*, *Phys. Rev. C* **94**, 024332 (2016).
 - [11] N. Nakatsuka *et al.*, *Phys. Lett. B* **768**, 387 (2017).
 - [12] D. Vretenar, N. Paar, P. Ring, and G. A. Lalazissis, *Nucl. Phys. A* **692**, 496 (2001).
 - [13] N. Paar, D. Vretenar, E. Khan, and G. Colò, *Rep. Prog. Phys.* **70**, 691 (2007).
 - [14] T. Inakura, T. Nakatsukasa, and K. Yabana, *Phys. Rev. C* **84**, 021302(R) (2011).
 - [15] H. Nakada, T. Inakura, and H. Sawai, *Phys. Rev. C* **87**, 034302 (2013).
 - [16] P. Papakonstantinou, H. Hergert, V. Yu. Ponomarev, and R. Roth, *Phys. Rev. C* **89**, 034306 (2014).
 - [17] E. G. Lanza, A. Vitturi, E. Litvinova, and D. Savran, *Phys. Rev. C* **89**, 041601 (2014).
 - [18] F. Knapp, N. Lo Iudice, P. Veselý, F. Andreozzi, G. De Gregorio, and A. Porrino, *Phys. Rev. C* **90**, 014310 (2014).
 - [19] H. Lancman, A. P. M. Van Twestende, and H. D. Graber, *Nucl. Phys. A* **291**, 293 (1977).

- [20] T. N. Buti *et al.*, *Phys. Rev. C* **33**, 755 (1986).
- [21] T. Motobayashi *et al.*, *Phys. Lett. B* **264**, 259 (1991).
- [22] E. Tryggestad *et al.*, *Phys. Rev. C* **67**, 064309 (2003).
- [23] A. Leistenschneider *et al.*, *Phys. Rev. Lett.* **86**, 5442 (2001).
- [24] H. Baba *et al.*, *Nucl. Phys. A* **788**, 188 (2007).
- [25] H. Sagawa and T. Suzuki, *Phys. Rev. C* **59**, 3116 (1999).
- [26] M. Wiedeking *et al.*, *Phys. Rev. Lett.* **94**, 132501 (2005).
- [27] P. Papakonstantinou, V. Yu. Ponomarev, R. Roth, and J. Wambach, *Eur. Phys. J. A* **47**, 14 (2011).
- [28] S. Ebata, T. Nakatsukasa, and T. Inakura, *Phys. Rev. C* **90**, 024303 (2014).
- [29] T. Inakura, H. Imagawa, Y. Hashimoto, S. Mizutori, M. Yamagami, and K. Matsuyanagi, *Nucl. Phys. A* **768**, 61 (2006).
- [30] J. Bartel, P. Quentin, M. Brack, C. Guet, and H. B. Håkansson, *Nucl. Phys. A* **386**, 79 (1982).
- [31] M. Kortelainen, J. McDonnell, W. Nazarewicz, P.-G. Reinhard, J. Sarich, N. Schunck, M. V. Stoitsov, and S. M. Wild, *Phys. Rev. C* **85**, 024304 (2012).
- [32] E. Chabanat, P. Bonche, P. Heenen, J. Meyer, and R. Schaeffer, *Nucl. Phys. A* **635**, 231 (1998).
- [33] A. Akmal, V. R. Pandharipande, and D. G. Ravenhall, *Phys. Rev. C* **58**, 1804 (1998).
- [34] D. R. Tilley, H. R. Weller, and C. M. Cheves, *Nucl. Phys. A* **564**, 1 (1993); <http://www.nndc.bnl.gov>.
- [35] A. Bohr and B. Mottelson, *Nuclear Structure* (Benjamin, New York, 1969).
- [36] M. N. Harakeh and A. E. L. Dieperink, *Phys. Rev. C* **23**, 2329 (1981).
- [37] B. Roth and K. Wildermuth, *Nucl. Phys. A* **20**, 10 (1960).
- [38] H. Horiuchi and K. Ikeda, *Prog. Theor. Phys.* **40**, 277 (1960).
- [39] F. Nemoto and H. Bandō, *Prog. Theor. Phys.* **47**, 1210 (1972).
- [40] Y. Suzuki, *Prog. Theor. Phys.* **55**, 1751 (1976); **56**, 111 (1976); **64**, 2041 (1980).
- [41] Y. Fujiwara, H. Horiuchi, K. Ikeda, M. Kamimura, K. Katō, Y. Suzuki, and E. Uegaki, *Prog. Theor. Phys. Suppl.* **68**, 29 (1980).
- [42] R. A. Baldock and R. A. Stratton, *J. Phys. G* **11**, 515 (1985).
- [43] P. Descouvemont, *Phys. Rev. C* **44**, 306 (1991).
- [44] M. Kimura, T. Suhara, and Y. Kanada-En'yo, *Eur. Phys. J. A* **52**, 373 (2016).
- [45] R. J. deBoer, J. Görres, G. Imbriani, P. J. LeBlanc, E. Uberseder, and M. Wiescher, *Phys. Rev. C* **87**, 015802 (2013).
- [46] I. Stefan *et al.*, *Phys. Rev. C* **90**, 014307 (2014).
- [47] R. K. Bansal and J. B. French, *Phys. Lett.* **11**, 145 (1964).
- [48] L. Zamick, *Phys. Lett.* **19**, 580 (1965).
- [49] M. V. Stoitsov, J. Dobaczewski, W. Nazarewicz, S. Pittel, and D. J. Dean, *Phys. Rev. C* **68**, 054312 (2003).
- [50] S. Ebata (private communication).
- [51] N. Furutachi, M. Kimura, A. Doté, Y. Kanada-En'yo, and S. Oryu, *Prog. Theor. Phys.* **119**, 403 (2008).